Exploring short-term trends in muon flux data using the CosmicWatch detector

Nevena Cail

Texas A&M University-Corpus Christi

May 6, 2025

Abstract. This study aims to collect data that may reveal correlations between secondary cosmic ray flux and space weather variables using the CosmicWatch muon detector. Cosmic rays (CRs) are high energy charged particles that penetrate into the solar system from across and beyond the galaxy. If, scattering through the solar wind and interplanetary magnetic field (IMF), they manage to reach Earth and bombard its atmosphere, CRs generate showers of secondary particles. Muons, known as "heavy electrons," make up a significant portion of these. Muons are born from the showers originating in the upper atmosphere and can often be detected at ground level before decaying. The CosmicWatch muon detector is a portable device developed at MIT as a project for physics undergraduates to collect and analyze their own muon flux data. A combination of spectral analysis of the muon counts and correlational analysis against space weather variables provides an exploratory study comparing well-understood expected relationships to what is easily extracted by our methods that use minimal data treatment. Restricted to a small data set, our correlation findings are subject to broad interpretation. The strongest results are on short timescales such as the presence of a diurnal variation in the muon count, and indications of transient space weather events such as geomagnetic storms.

1. Introduction

1.1 Cosmic rays

Cosmic rays (CRs)–as summarized from Sharma (2008)–are high energy ionized particles that are produced by various (and mysterious) cosmic accelerators, such as supernovas, and arrive to us from across and beyond the galaxy. The variations in flux of CRs at Earth, and their trajectories through the heliosphere has been extensively studied and quantified over the last century. CRs experience a wide range of modulation that increase or decrease their flux at Earth. The largest sources of modulation come from the solar wind and magnetic field structures in the heliosphere that vary with solar activity, and interaction with Earth's magnetic field. Many signals in CR flux are cyclical and exist on both short and long-term timescales, on the order of days to decades. Transient events such as from explosive solar activity can also modulate the flux over short periods of time, but these events averaged over time contribute to long-term periodicities in CR flux variations.

CR data collection comes in several forms. Low energy CRs will be absorbed by particles in the atmosphere, but can be detected above or in the upper atmosphere by space weather instruments. Ground-based detectors can measure the flux of CR secondaries that travel to Earth's surface. Secondaries are secondary particles of CRs formed in a cascading particle "air shower" when high energy CRs are incident on molecules in Earth's atmosphere. The number of particles that reach Earth depends on the energy of the incident CR, but the muon flux at sea level is typically estimated as one per square centimeter per minute. The initial particles that result from these reactions are pions and kaons. Pions rapidly decay into muons, neutrinos, and gamma rays. Most secondaries that are detected at ground level are muons. CRs can be studied directly by their detection above the atmosphere such as by instruments on satellites, or by detection of their secondaries measured at ground level by muon telescopes and neutron monitors.

1.2 CosmicWatch muon detector

The CosmicWatch muon detector was developed at Massachusetts Institute of Technology in 2018 as a project for undergraduate physics students to explore CR phenomena, and collect and analyze their own data with a portable and inexpensive detector. We summarize the mechanism of the detector and relevant considerations about the data collection from the CosmicWatch physics paper (Axani 2019) here.

The detector uses a scintillator block as the detection medium for particles to pass through. The block is an organic transparent plastic with added fluorescing dopants. Energy deposited in the block by particles will be re-emitted as electromagnetic radiation, causing the block to fluoresce. The scintillator slab is coupled to a silicon photomultiplier microchip (SiPM). Photons incident on the SiPM will cause a

Geiger discharge, creating a small amount of current proportional to the number of incident photons. This signals a particle detection, and the produced current is routed through the PCB to amplify and shape the signal so it can be measured by the Arduino Nano microcontroller.

Important considerations about the functionality of the detector are measured and thoroughly explained by Axani (2019). These include: assembling the scintillator-SiPM coupling to maximize internal reflection in response to a particle event, and to minimize background noise (ambient or other sources of light other than the scintillator), as well as the calculated deadtime of the detector due to the slowness of the Arduino.

The most purified count results are expected when operating two detectors simultaneously, or in coincidence mode. In coincidence mode, two detectors are connected with a cable and will only register an event if both detectors trigger simultaneously (within a small time window determined by the connecting cable used). Coincidence mode events are most likely to be cosmic ray muons because a typical muon will deposit 2 MeV of energy in the scintillator without being deflected such that if its angle of incidence allows it to pass through both detectors, it will likely trigger them simultaneously. And this is not likely to be the case for other kinds of radiation due to high chances of scattering and loss of energy.

1.3 Modulation of CRs

Determining the state of Earth's heliosphere, magnetosphere, and atmosphere is based on the measurement of CR variations, both by direct measurement of CRs in the upper atmosphere and of CR secondaries—primarily muons. Data from these experiments have been widely used to study CRs trends over the course of solar cycles (Potgieter 2013), and allowed for many modulation sources increasing or decreasing CR flux to be observed. CR flux is dominated by galactic CRs, as opposed to solar CRs. Solar CRs are typically of too low energy for ground-based detectors to respond. Therefore, solar activity acts more strongly as a modulator of CRs than as a source, although relativistic solar particle events associated with explosive solar ejections can dominate galactic CRs on short timescales (Pomerantz and Duggal 1974). We summarize modulators of galactic CRs here.

1.4 CR modulation in the heliosphere

The flux of CRs is influenced by magnetic deflection and diffusion (particle scattering) in interplanetary space. The interplanetary magnetic field (IMF), carried by the solar wind and co-rotating with the Sun (in a Parker spiral), alters the trajectories of solar system-bound CRs through scattering and diffusion effects, shielding their penetration into the solar system (Jokipii 1966; Potgieter 2013). This happens by the acceleration or deceleration of CRs from ion streams emanating from the Sun, carrying magnetic fields, and the diffusion of CRs through magnetized clouds. These combined effects were formulated by Parker (1965) in his solar modulation theory. The result is that CR anisotropies are created throughout the heliosphere, such that they do not come to Earth equally from all directions. During periods of high solar activity, increased solar wind speed and stronger magnetic fields increase CR scattering and outward convection, reducing their flux at Earth.

One periodic contributor to variation in the solar wind is the rotation of the Sun. The Sun rotates every 27 days, which regularly changes the position of coronal holes with respect to Earth. Coronal holes are regions of open magnetic field lines, which serve as sources of high-speed solar wind streams (Richardson and Cane 2004) that can modulate the CR flux at Earth. When these high-speed streams interact with slower solar wind regions, they create co-rotating interaction regions (or CIRs) which rotate with the Sun's rotation and can therefore be repeatedly observed. This enhances CR scattering thereby reducing CR flux (Heber, Sanderson, and Zhang 1999).

There is also a diurnal variation of CR flux that occurs due to Earth's rotation. The following is a summary of related details from Swinson, Regener, and John (1990). Every day, a CR terrestrial telescope observes with the greatest elevation above and below the ecliptic plane at 18:00 and 06:00 sidereal time, respectively, due to the axis tilt of the Earth. Therefore, components of the CR signal perpendicular to the ecliptic plane will obtain a maximum at these times. This is a purely geometric effect which samples the CR North-South anisotropy every day. From this data, it is observed that the best correlation of the diurnal CR flux signal variation is with the IMF one day later. The signal itself is driven by the optimal alignment of the Earth's magnetosphere and the IMF, which occurs once daily at 18:00 sidereal time (Parker 1967). The magnitude of this contribution to the daily variation is second only to that from the 27-day solar rotation.

1.5 Solar activity modulation of CRs

Solar activity and its variations throughout the 11-year solar cycle cause periodic fluctuations in CR flux.

Throughout the solar cycle, the number of observed sunspots and coronal mass ejections (CMEs) fluctuates from a minimum to maximum level of solar activity. Additionally, every solar cycle, the magnetic field of the Sun reverses near the solar maximum. Therefore, the Sun completes the solar magnetic cycle when it returns to its original polarity every 22 years, creating another long-term signal in the CR flux. Propagating diffusive barriers in the outer heliosphere formed from interactions between the solar wind and magnetic field cause large, long-term steps in CR flux when they occur with a higher rate over the course of the solar cycle (Potgieter 2013). During the solar minimum, these effects are reduced so more galactic CRs penetrate to the inner heliosphere, increasing the CR flux.

Transient events such as CMEs have the potential to generate Forbush decreases if they envelop Earth. Forbush decreases are a decrease in CR flux caused by increased deflection of CRs, since the enveloping CME acts as a diffusive barrier. It is also possible for CMEs located at large distances from Earth's orbit to decrease CR flux in a specified direction (Barbashina et al. 2007) by altering the IMF structure. However, impacting CMEs also strengthen the ring current around Earth which weaken the Earth's magnetic field. This is associated with geomagnetic storms. The frequency of these events correlates with the solar cycle.

1.6 Atmospheric modulation of CR muons

Once CRs have arrived at Earth, atmospheric interactions can modulate their produced muons, as their survival is affected by variations in temperature and pressure. These effects are summarized here, from Mendonça et al. (Dorman, 2004, as cited in 2013). Muon survival probability depends on the density and altitude of the atmosphere. Higher temperatures cause the atmosphere to expand such that the muon-producing pions are created higher in the atmosphere, increasing the distance they have to travel to Earth's surface. This increases their chance of decay before they reach ground level, reducing the muon flux. Lower temperatures, in turn, enhance their likelihood of interaction before decay, increasing flux. The temperature effect on CR flux results in a seasonal variation overall.

The pressure effect refers to how atmospheric pressure changes the density of air, affecting the mean free path of CR secondaries. An increase in atmospheric pressure corresponds to an increase in the number of air molecules, which leads to greater absorption and scattering of secondaries, thereby reducing muon flux at ground level. Conversely, lower atmospheric pressure leads to a relative increase in observed flux.

Since these atmospheric effects are local effects modulating the CR secondary's incidence on a ground-based detector, and not CR arrival to Earth itself, they are necessarily removed in CR studies since they are background signals impeding understanding of CRs in the solar system.

2. Methodology

2.1 Data

The CosmicWatch muon count (MC) data we collect is contiguous from February 27—March 20, 2025 and March 25—April 19, 2025. These are periods of 21 and 25 days, respectively, which we will refer to as data set 1 (D1) and data set 2 (D2). This data set is undesirably small but could not be gathered over a longer time due to various difficulties with the consistency of the detector to stay powered on and continuously write data. Therefore, we are restricted to analyzing short-term variability in the MC signal as opposed to long term trends. This data is binned hourly and daily. The hourly data is used for spectral analysis and harmonic fitting, and the daily data is used in a raw correlation calculation against several chosen space weather variables (SWVs).

We operate only a single detector instead of in coincidence mode. Therefore, we expect a significant contribution of the signal to be background noise rather than purely from muon events. There is the added benefit, however, that no muon events are eliminated when using a single detector. This could happen in coincidence mode if the incident angle of the muon does not give it a trajectory through both detectors. We use a Python program to read the serial data from the detector Arduino to save the computer time of the event, and write the data continuously to a CSV.

Proper data handling of the MC would involve correcting for atmospheric variations such as the temperature and pressure effects to zero local influences and reveal the true behavior of galactic CRs (Forbush 1937; Mendonça et al. 2013). Our approach instead embraces the raw data, which may require careful interpretation of ambiguous results since they are likely to capture noise from these effects. There is the potential added benefit, however, that not eliminating these effects actually preserves information about the atmosphere as it is impacted by space weather. Strong solar wind and CMEs should affect the temperature and pressure of Earth's atmosphere, and this may be reflected in our MCs. By zeroing the atmospheric correlation, we might remove the very phenomena we wish to capture.

The SWVs we correlate with the MC is downloaded from NASA's OMNI database. These historical data are IMF magnitude (nT), solar wind speed (SWS), or the solar plasma speed (km/sec), R sunspot number (R SNo.), and solar index F10.7 (sfu)—a measure of solar radio flux; an excellent indicator of solar activity. We download daily averages of each for the time period of the MC data. Each of these variables can be linked to or directly impact CR flux. OMNI data uniquely marks invalid values which we remove in a preprocessing step.

Data from OMNI are primarily collected from spacecraft located at L1, upstream from the Earth to the Sun, and are time-shifted by 40-60 minutes to account for solar wind propagation from L1 to Earth. This gives the data at reached-Earth's-bow-shock time instead of L1 time. Therefore, we do not have to manually account for this delay in our procedure.

2.2 Spectral analysis

Independent of the SWVs, we do spectral analysis of the MC signal using a Fast Fourier Transform (FFT) implemented via SciPy (Virtanen et al. 2020) and wavelet analysis using PyWavelets (Lee et al. 2019), to extract its periodic components, and identify transient events. Any periodicities in our data are restricted by the length of our contiguous data sets to short term signals such as diurnal variations.

The FFT and wavelet scalogram complement each other. The FFT can identify frequencies present in a signal, but assumes they are global, so will struggle to reconstruct a signal if frequency content changes over time. The wavelet transform can be used to detect the location in time of frequencies which is useful for identifying transient events. Explosive solar events, for example, will modulate the CR flux over a period of a few days as characteristic of a Forbush decrease. It is also possible for a high energy proton event to overwhelm the galactic CR signal. These events should occur on short timescales, creating hotspots in the wavelet transform scalogram at the event's corresponding periodicity. But this analysis will only show the power of periodicities in the MC signal at locations in time, without indicating what the relative values of the MC are. We do some supplementary, non-rigorous documentation of space weather event monitoring from spaceweather.com, and atmospheric conditions from Meteostat.net to classify hotspots on the scalogram. We also calculate a simple rolling average on the MC as an estimate of the expected count rate to gain insight into MC behavior at the scalogram hotspots. Finally, we corroborate the strongest frequencies across the FFT and wavelet analysis.

The FFT is done on hourly detrended MC data. Generally, finer sampling intervals improve the statistical focus on frequencies in the data. However, a general note is if the sampling interval is decreased too much, then each bin will not contain a statistically meaningful value. For a Poisson variable like radiation event counts (occurring independently of each other with a constant average rate), the square root of the counts per time interval–the Poisson noise–should be relatively small. If it is relatively large due to a smaller than physically applicable sampling interval, then the signal is dominated by random fluctuation instead of the underlying, more long term representative behavior. Conversely, if the sampling interval is too large, then higher frequency signals exceeding the Nyquist frequency (1 per twice the sampling interval, or half the sampling rate) are either lost or "alias" into low-frequency peaks. This means that fluctuations occurring on timescales faster than the Nyquist frequency contribute to a background noise that folds into the low frequency components in the FFT. A similar effect can be observed when performing an FFT on data that has not been detrended, which is that the constant background signal causes the FFT to be dominated by a peak that blows up at 0 Hz. We detrend the MCs simply by subtracting all values by the average.

For the wavelet transform, we use a Morlet wavelet with a bandwidth of 1.5 and central frequency of 1.0. These parameters customize the wavelet that is passed over the data, and are suited to most purposes. Since our data set exists only on the order of weeks, we place emphasis on finding signals likely caused by solar and geomagnetic disturbances by using wavelets of 100 scales, with 2 to 72-hour widths, progressing logarithmically (by (1), using central frequency $f_c = 1.0$ directly translates scales to hours). Logarithmic spacing of the scales allows for more balanced sampling of the frequencies. Linear spacing of the scales would cause oversampling of high frequencies and undersampling of low frequencies.

$$T = s\frac{\delta t}{f_c} \tag{1}$$

Period T of the analyzing wavelet is in units of the sampling interval δt and equal to scale s multiplied by a factor related to the central frequency f_c of the wavelet used.

A key feature of time-frequency analysis is the time-frequency uncertainty principle, or the trade-off between resolution in frequency and time. Scales are proportional to oscillation period with units of the sampling interval of the data (1), and determine the

width of the analyzing wavelet. Larger scales corresponding to wider wavelets therefore can resolve lower frequencies by taking in a larger swath of the time series. The trade-off is that although they have higher resolution of these lower frequencies, they have poorer resolution in time of when a feature happened. Therefore, if plotting of the scalogram were to reflect true bandwidth differences, then as scales increase further up on the y-axis of a scalogram, the resolution decreases horizontally since each power of the signal component displayed must correspond to a larger length of time (x-axis). Conversely, smaller scale wavelets have better timing resolution but less certainty about the high frequencies, would cause pixels to appear more vertically stretched (capturing a broader range of frequencies at that time). However, most plotting is typically done in log scale so all pixels are uniform, which does not visually represent the underlying trade-offs.

Another property are edge or boundary effects of wavelet transforms which can mislead interpretation of the results, so we include the cone of influence on our scalograms. This indicates where edge effects are significant. Edge effects arise because each wavelet (of each scale, or width) convolves the data centered at each data point. Therefore, the wavelet is not always fully within the time domain of the data set towards the edges of the time series. At larger scales, edge effects are most prevalent because the wavelet is widest and therefore is evaluating the frequencies beyond the edges of the data set at each end the longest.

2.3 Harmonic fitting

One treatment of the hourly MC used is fitting it to a single harmonic (2) for each 24-hr period (Abdullrahman, Hya, and Aied 2025).

$$f(t) = A + B\cos(\omega t + \phi) \tag{2}$$

Here, A is the offset, B is the amplitude, and ω is the angular frequency given by $\omega = 2\pi f$. The frequency f is assumed to be $1/24\text{hr}^{-1}$ since the fit is applied to one day of hourly data at a time. The variable t represents the hour of the day, ranging from 0 to 23, and ϕ is the phase angle of the cosine wave peak. The ratio ϕ/ω gives the lateral shift of the wave to the left. We also compute the coefficient of determination R^2 as a measure of the quality of the fits.

By applying a daily harmonic fit to the MC, we can extract daily amplitude and phase angle values. These can be correlated to the values of the other SWVs over many days to indicate a positive or inverse relationship by value, and their synchronized or time-lagged relationship temporally.

A double harmonic fit is preferred for the diurnal variation of muon data (Mailyan and Chilingarian 2010), but this is with the assumption that the data has atmospheric corrections applied. Since this is an exploratory study, we prioritize keeping the data as raw as possible, and the fit as simple as possible. The single harmonic fit serves simply as an additional metric for contributing to exploration of ground-level muon data and examining the contrast of modulations that are well-established and expected, versus what we can easily extract. Despite possible noise over-fitting of MC from the simplicity of the fit and data treatment, we may still be able to compare the clustering of the resulting amplitudes and phases of MC as they vary with SWVs, and establish trends between them.

2.4 Correlation analysis

We do scatter plotting of the hourly MC versus hourly temperature and pressure, retrieved from Open-Meteo for the approximate latitude-longitude location of our detector, to get a sense of the significance of this relationship in our data. Additionally, Pearson and Spearman coefficients are calculated to measure the strength of linear and monotonic relationships, respectively, of the daily amplitudes of the MC with the daily-averaged values of the SWVs. Data which is elliptical causes Pearson and Spearman coefficients to be similar, and the Spearman coefficient is more disturbed by outliers than Pearson. We also look at these correlations using the raw daily MC. We also want to correlate the MC phase (converted to UTC Peak Hour) to the SWVs. However, Peak Hour is a circular variable while the SWVs are linear, so circular-linear correlation (Mardia's method implemented in the pycircstat Python library) is used to calculate the correlation coefficient. Because the data set is small, correlations may arise by coincidence or otherwise be misleading, so we use bootstrapping as a way to measure how representative our sample is of its population. This technique recalculates the coefficients by resampling with replacement a large number of times to get the average value and error (standard deviation). Finally, we shift the SWVs (with a special interest in the IMF) one day forward to see if any of the correlations strengthen. This is because we expect SWVs to lead the MCs, meaning there should be some delay for MCs to respond to changes propagating in the heliosphere. It is possible that one day is too much or too little of a time shift to represent the cause and

effect relationship of the variables, and instead puts them closer to being out of phase, causing a drop in correlation strength with MC.

3. Results

3.1 Spectral analysis

We make some preliminary observations on both hourly MC data sets by plotting the raw data as a time series (Figure 1), and in a histogram (Figure 2). The raw data has clear minimums and maximums, of similar magnitudes between both data sets. We make note of these time periods where the signal is significantly disturbed such that the MCs register as outliers according to their determination by the interquartile range method, highlighted in Figure 2. Outliers by this method are MCs exceeding 2438 and below 2238. The data points when this occurred are listed in Table 1.

Figure 2 shows that the hourly MCs (aggregated over both data sets) approximate a Poisson variable. Poisson distributions do not have outliers, so the fact that outliers exist in the MC data tells us the MC per hour is not constant on average. Binning by a smaller sampling interval would likely converge on a fit to a Poisson distribution. The variations due to hourly binning causes outliers because the count rate per hour is evidently not stable (or constant) over time (or, on average). However, the symmetry of the histogram (the mean=2339.42, and median=2338.00 show the data is negligibly skewed) lends to the Poisson nature of the counts despite the non-constant average event rate. Whether we can classify our variable as Poisson is useful to know because it can guide decisions on how best to bin the data for FFT analysis. The closer we can get our data to a Poisson variable, such as by reducing the sampling interval (while monitoring the increasing Poisson noise), the less aliasing we would have the in the FFT. For convenience, we simply note these observations in the MC distribution for later interpretation of the FFT, and continue using hourly count data for the spectral analysis.

The FFT performed on each data set are shown in Figure 3 and Figure 4. Looking between the results for each time period, we see that the FFT for the longer data set D2 converges on the physical 24-hr value (23.96) that emerged in the FFT from the shorter datatset D1 (23.90). This is an expected result for muons that should correspond to diurnal atmospheric modulation caused by night and day. The ˜12-hr period peak (11.98) also dominates in the FFT from D2, and it is also a noticeable peak in the FFT of D1. This is a twice-daily variation in the MC, which could be due to two opposite and extreme orientations of Earth (and its magnetosphere) in its rotation relative to the IMF, allowing the CM to peak twice per day. This periodicity also echoes back to Swinson, Regener, and John (1990) which stated that a detector maximally surveys the North-South CR anisotropy twice daily. Most likely, this is caused from atmospheric pressure having a semi-diurnal variation. Additionally, the 251.00-hr and 502.00-hr peak from D1's FFT, and 551.00-hr peak from D2's FFT correspond to approximately half the length of D1, full length of D1, and full length of D2, respectively. These large periodicites are likely misleading peaks in the FFTs caused by aliasing of higher frequency components (shorter than the Nyquist frequency of 1 per 2 hours) into lower frequency components such as these. Because the periods are on the order of the total time domain of the signal, they are suspicious and can be ignored. Decreasing the sampling interval to 5-minutes (to obtain 5-minute MCs from D2), which we can assume makes the data more Poissonian, helped to converge the strong periodities closer to 12 and 24 hours (Figure 4b). It is unlikely that the 5 minute count rate would still cause aliasing, so this conveys there may be slow varying background radiation levels or noise causing a similar artifact, and so perhaps removing this in a more sophisticated way than simply subtracting out the average would help refine these results.

Scalograms are generated for both data sets as well which show how frequencies in the MC signal change over time (Figure 5). The FFT works well if periodicities are present in the signal globally, but stumbles if frequencies are transient or non-constant. This is where the wavelet analysis can compensate for and corroborate the FFT results.

We notice changes in the appearance of the scalogram as we look from small to large scales. At small scales, the wavelets are resolving higher frequencies which tend to exist oh short timescales. There is more fluctuation in the signal on these scales

For D1, the scalogram (Figure 5a) displays that the most powerful signals occur at the ˜24-hr frequency from its corresponding FFT. There also appears to be a wide range of lower frequencies, possibly amounting to a disturbance of the signal in the time period March 4–March 8, 2025. Checking the plot of the expected MC rate (Figure 6a), we see that this disturbance appears to correspond with an extended decrease in counts with a slow recovery, causing the lower frequency hotspots in the scalogram. We also notice the outlier occurring on March 3 corresponds to a momentary loss of the twice-daily frequency component on the scalogram, indicating that

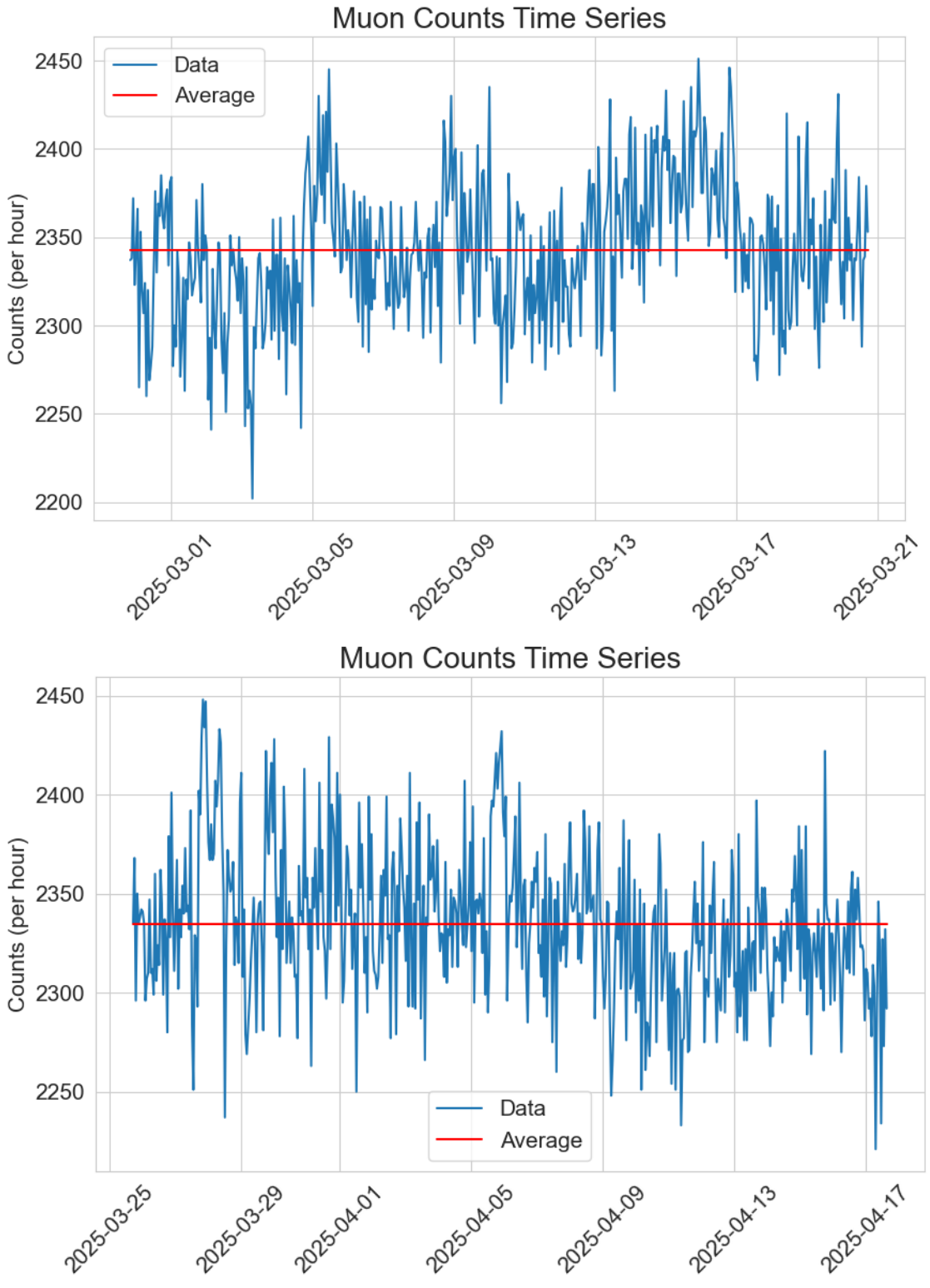

Figure 1: Raw hourly muon count time series from both data sets.

Table 1: Outliers in the hourly muon count (MC) data: MC < 2238 and MC > 2438.

Timestamp (UTC)	**MC**
MC $<$ 2238	
2025-03-03 07:00:00	2202
2025-03-28 12:00:00	2237
2025-04-11 09:00:00	2233
2025-04-17 07:00:00	2221
2025-04-17 11:00:00	2234
MC $>$ 2438	
2025-03-05 11:00:00	2445
2025-03-15 22:00:00	2451
2025-03-16 19:00:00	2446
2025-03-27 20:00:00	2448
2025-03-27 22:00:00	2447

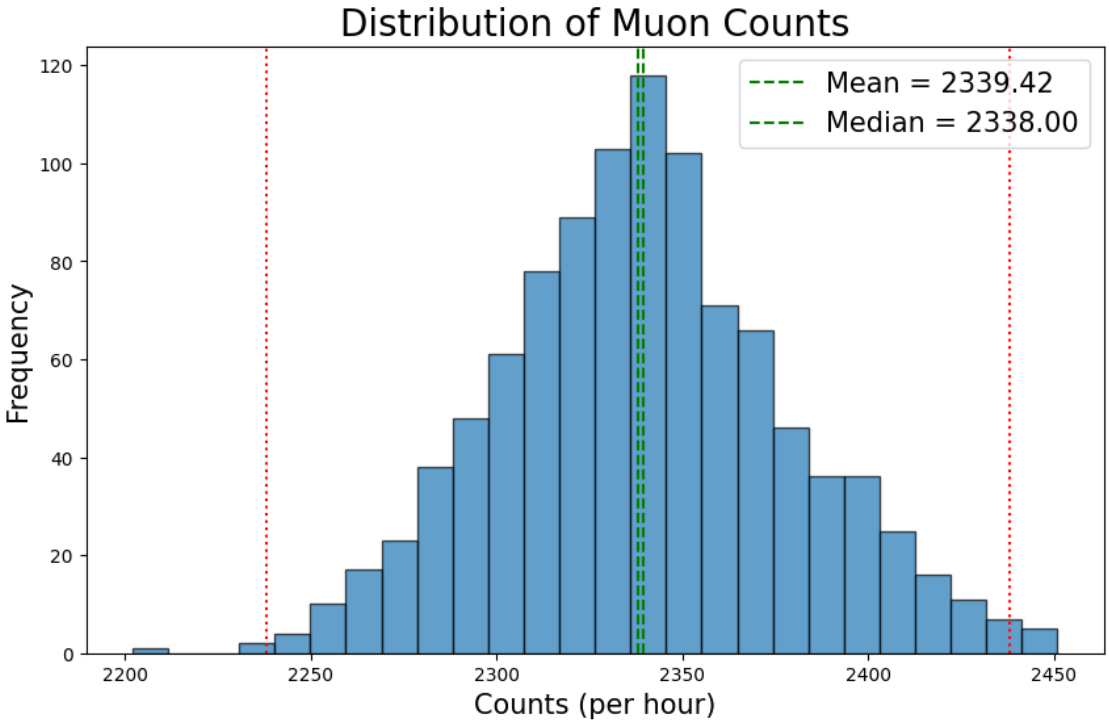

Figure 2: Histogram of hourly muon counts aggregated across both data sets. Red lines indicate the lower and upper bounds for detecting outliers. The mean and median are drawn to indicate any skew of the data.

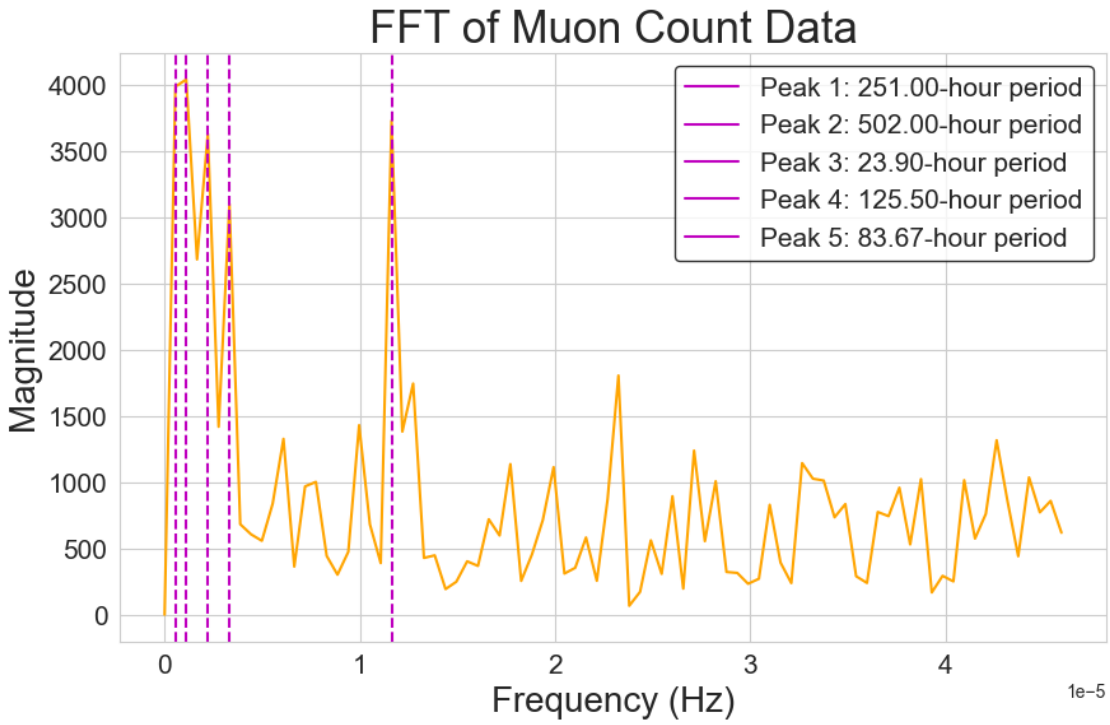

Figure 3: Fourier analysis of data set 1. The vertical dashed lines highlight the five largest peaks, listed in descending order, and labeled by the period in hours equal to the inverse of the frequency.

the signal may have been disrupted, which lends to its relatively low power on the D1 FFT. Similarly, the disturbance previously identified corresponds to a blackout of the ˜24-hr signal component. Geomagnetic storm monitoring news from spaceweather.com on March 5 described that a CME had passed near Earth, and should cause a minor geomagnetic storm. This could explain the slow drop in MC in the days after the MC peak on March 5. The scalogram for D2 (Figure 5b) noticeably has a hotspot on March 29 between scales 40 and 50. Occurring after this is a dampening of the ˜24-hr component. This, together with the upward spike and plummet on Figure 6b signals a disturbance to the typical MC. $\lambda(t)$ also dips and lingers below the average count rate after April 5. Positive spikes in the MC may be due to optimal atmospheric conditions. Graphical data from Meteostat.net for the Corpus Christi International Airport location showed there was low but rising pressure on April 5, coinciding with falling temperatures. This recovery from a low pressure system combining low pressure with low temperature could have provided a transitional period of minimal resistance to muons. Spaceweather.com reported on April 14 reported that two CMEs would impact Earth on April 16, causing a G2 level storm. This latter event would explain that the smallest MC value in D2 is achieved the following day.

If these correlations with geomagnetic storms are truly reflected in our untreated muon data, then we can glean something about the temporal relationship between the storms and their manifestation in the MC, which is that when the geomagnetic storm is taking place, the counts tend to decrease over the course of the following day, and recover back to average values in 2-3 days. This roughly corroborates the known patterns of Forbush decreases. The curiosity is the seemingly anticipatory spike in counts, as previously mentioned, before these events. This could be the coincidence of convenient atmospheric conditions for muon penetration, or point to how an incoming CME deforms the IMF such that CRs get less deflected in the intervening space, and increase in flux at Earth.

3.2 Correlation analysis

The hourly MC (from both data sets combined) correlations with temperature and pressure shown in Figure 7 appear slightly positive and negative, respectively. Strong negative correlations were expected for both because lower temperatures and lower pressure provides lower resistance to muon travel, so this could

Figure 4: Fourier analysis of data set 2. (a) Muon counts binned by 1 hour. (b) Muon counts binned by 5 minutes. The vertical dashed lines highlight the five largest peaks, listed in descending order, and labeled by the period in hours equal to the inverse of the frequency.

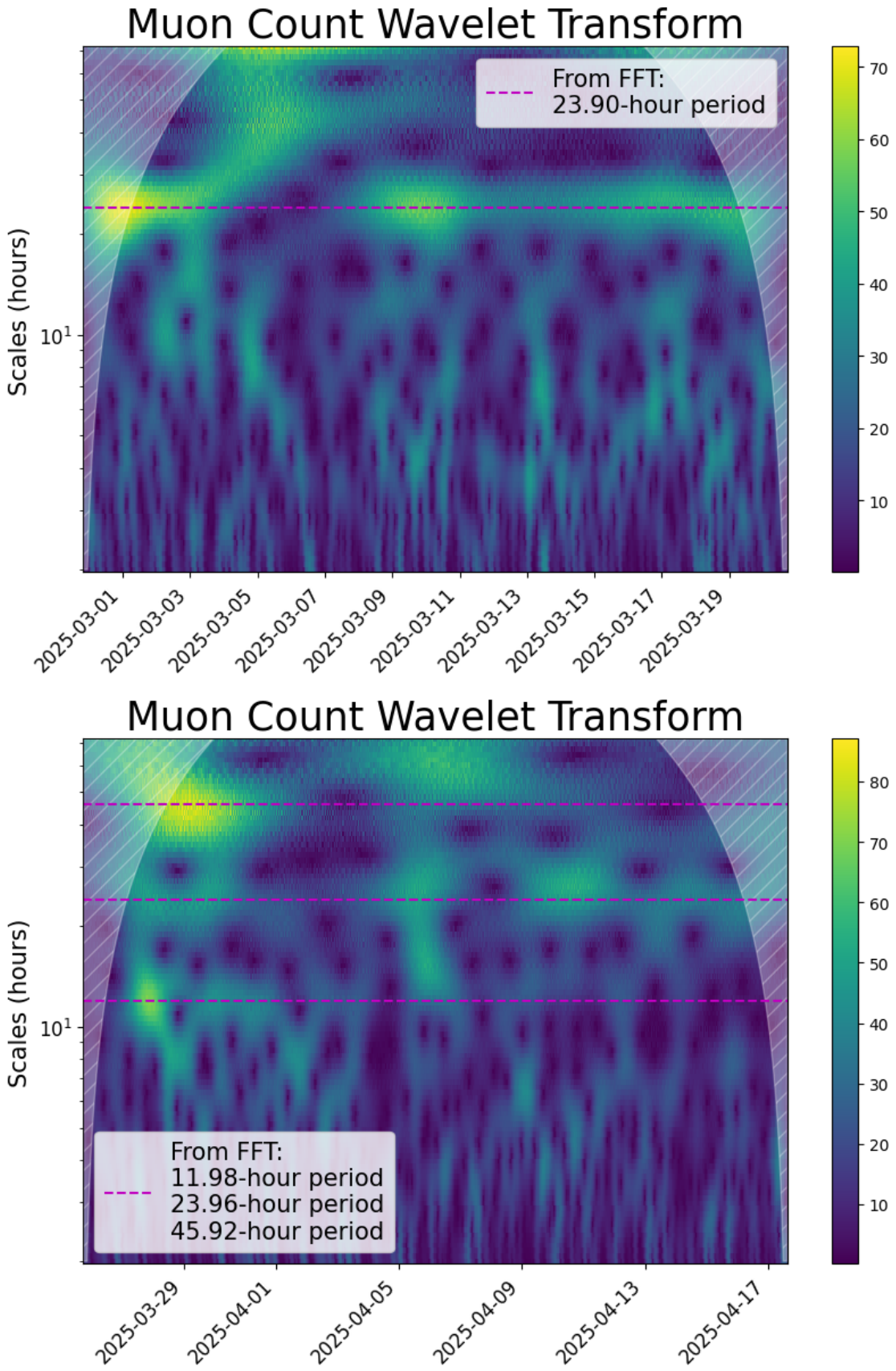

Figure 5: (a) Data set 1. (b) Data set 2. Wavelet analysis of the hourly muon count data sets. Significant peaks from the FFTs are drawn to highlight corroborating results from the wavelet transform.

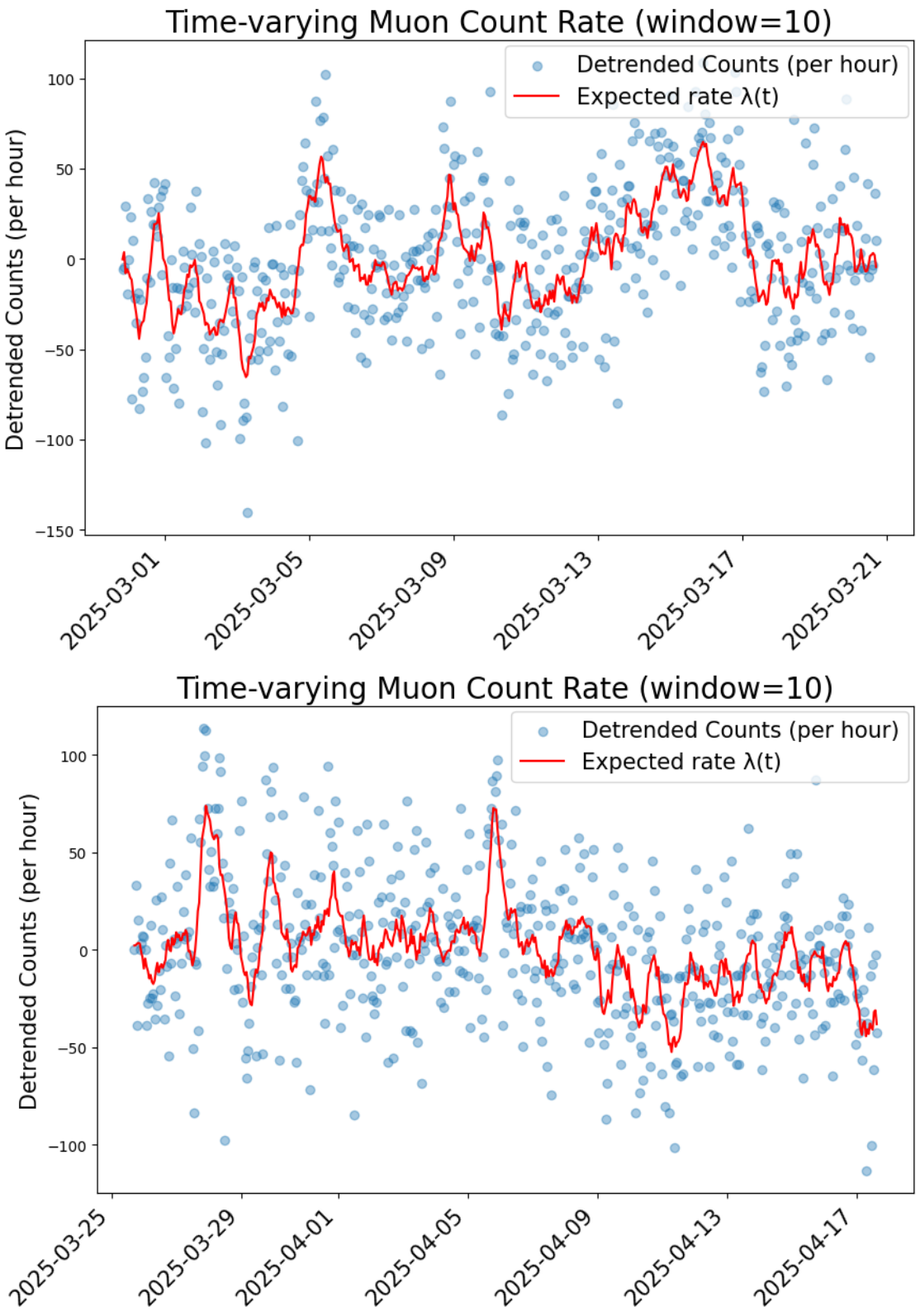

Figure 6: (a) Data set 1. (b) Data set 2. Calculated expected muon count rate $\lambda(t)$ for both data sets by taking the rolling average with a window of 10 hours.

convey some information about the amount of noise in our signal. Higher temperatures may be directly positively influencing the sensitivity of the detector if the detection mechanism is more dependent on heat than was realized. Because of the prominent presence of the 12 and 24-hour periodicities found in the MCs from the spectral analysis, it is reasonable to assume that the fluctuations of temperature and pressure should be causing the correlations illustrated by Figure 7. The fact that the muon count correlation is only negative with pressure conveys that the pressure effect is dominating over the temperature effect in our data. Meaning that we could reason what is happening is higher temperatures, which cause the warm air to rise and leave behind a region of lower pressure are both causing higher muon counts. So this explains both correlations and suggests that temperature is just an accessory to the pressure effect. We could further reason that MC correlation with semi-diurnal pressure variation rides on the diurnal temperature variation, ultimately making the temperature correlation more noisy and the pressure correlation relatively stronger.

The correlation analysis between daily MCs and daily-averaged SWVs in Table 2 lists the Pearson (P) and Spearman (S) correlation coefficients. Due to removal of invalid values in the SWV data, the length of the data sets available for correlation calculation varies across the variables. Generally, smaller data sets align with increased uncertainty, and these effects are pronounced since the span of the MC data was small to begin with (˜6 weeks from combining D1 and D2). Physically, indicators of solar activity should cause lower CR flux, but none of the SWVs show a strong negative correlation. The most statistically significant value was the correlation with F10.7 ($P = 0.29 \pm 0.13, S = 0.28 \pm 0.14$). However, F10.7 varies little (8%) with respect to the average. So the hypothetically more dramatic effects on MC from atmospheric effects may be coincidentally coinciding with variations in F10.7, and it is unlikely this correlation is causal. Additionally, F10.7 is a widely used metric, but best for analyzing long term trends related to the solar cycle rather than short-term modulation. Correlation with SWS was also relatively strong and positive with $P = 0.21 \pm 0.13$. It is expected that higher SWS lowers CR flux, so the counter-intuitive positive correlation here might be explained by some special circumstances, especially given that the data sets are small and so do not capture long term trends that would average out these defects. One possibility is that in recoveries from Forbush decreases, the MC rises while the solar wind speeds up. If these events in our data are numerous enough, they may make up a significant portion of the time series, allowing these MC recovery phases to determine the correlation. Another circumstance is that high solar wind may have been suppressed from reaching Earth for some time when forming CIRs, and simply correlate with normal or rising MCs. The low correlation with IMF ($P = -0.06 \pm 0.18, S = 0.06 \pm 0.21$) lends itself to how IMF and MC might also be out of phase due to the delay in changes in the IMF manifesting in the MCs. Overall, the Pearson coefficients were stronger than Spearman, again conveying the noisiness of the data. The noise in the data could be dominated by the use of daily binning of the MCs which obscures MC variations occurring within the period of a day. Daily MCs were found to have a coefficient of variation of 1%, which will make correlation more unreliable in general.

The results for the harmonic fitting include average amplitude (19.89 MCs), circular average peak hour (14.33 UTC), and average R^2 of the fits (0.20). While interpreting the correlations between MC amplitude and daily-averaged SWVs in Table 3, we observe that the amplitude is really a measure of the fluctuation of the MCs in a day. An intended advantage of the harmonic fit is that is uses the hourly MCs instead of daily MCs which hide shorter time variations. Many of the fits are poor, which should dampen the amplitude for those days where R^2 is lowest. This means that these days did not have a prominent diurnal fluctuation to guide the fit. We might expect then, that if hourly MC is dominated by atmospheric effects, that influences on CRs by the SWVs could weaken or strengthen the fluctuation. The most statistically significant result was the strong positive correlation of SWS with MC amplitudes ($P = 0.49 \pm 0.13, S = 0.44 \pm 0.13$). This correlation likely arises from coincidental variation in confounding atmospheric variables, but could also be affecting the atmospheric conditions by increasing temperature in the upper atmosphere, lowering local pressure causing relatively more dramatic fluctuation of the MCs during the daytime–when the solar wind is impacting overhead.

The results for daily MC peak hour correlating to the SWVs (Table 4) were strongest for the IMF. This notably contrasts with the negligible correlation IMF had with MC amplitude. Stronger IMF could push the optimal local time for cosmic ray entry, thereby correlating with the peak time of MCs. But it is suspicious for there to be modulation of the peak hour by the IMF, but not the amplitude.

Table 2, Table 3, and Table 4 also list P and S for when the SWVs are shifted forward by one day. For

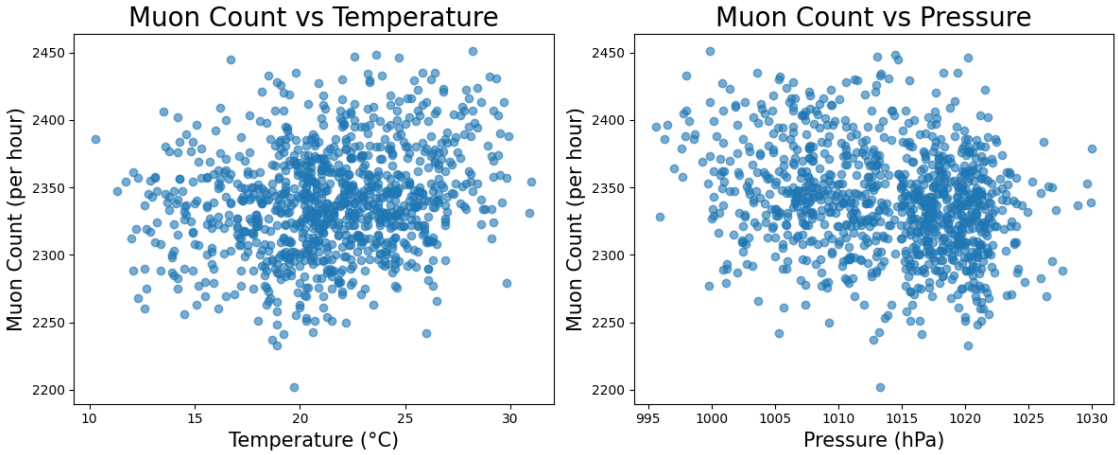

Figure 7: Scatter plots of hourly muon counts as they vary with hourly local temperature and pressure data (fetched from Open-Meteo).

Table 2: Pearson (P) and Spearman (S) correlation coefficients for daily muon counts versus current and one day forward shifted daily-averaged space weather variables.

Space Weather Variable	$P_{current}$	$S_{current}$	$P_{shifted}$	$S_{shifted}$
Interplanetary Magnetic Field	-0.06 ± 0.18	0.06 ± 0.21	0.24 ± 0.16	0.29 ± 0.20
Solar Wind Speed	0.21 ± 0.13	0.16 ± 0.15	0.00 ± 0.15	-0.02 ± 0.15
R Sunspot Number	0.26 ± 0.18	0.18 ± 0.21	0.19 ± 0.18	0.12 ± 0.21
F10.7 Index	0.29 ± 0.13	0.28 ± 0.14	0.27 ± 0.14	0.23 ± 0.15

Table 3: Pearson (P) and Spearman (S) correlation coefficients for daily muon count amplitudes versus current and one day forward shifted daily-averaged space weather variables.

Space Weather Variable	$P_{current}$	$S_{current}$	$P_{shifted}$	$S_{shifted}$
Interplanetary Magnetic Field	-0.08 ± 0.19	-0.11 ± 0.21	0.18 ± 0.26	0.08 ± 0.21
Solar Wind Speed	0.49 ± 0.13	0.44 ± 0.13	0.15 ± 0.16	0.15 ± 0.18
R Sunspot Number	-0.29 ± 0.18	-0.33 ± 0.20	-0.32 ± 0.21	-0.30 ± 0.20
F10.7 Index	-0.12 ± 0.15	-0.15 ± 0.16	-0.12 ± 0.15	-0.16 ± 0.17

Table 4: Circular-linear correlation coefficients r for daily muon count phase versus current and one day forward shifted daily-averaged space weather variables.

Space Weather Variable	$r_{current}$	$r_{shifted}$
Interplanetary Magnetic Field	0.30 ± 0.10	0.24 ± 0.13
Solar Wind Speed	0.22 ± 0.12	0.36 ± 0.17
R Sunspot Number	0.27 ± 0.13	0.25 ± 0.13
F10.7 Index	0.19 ± 0.10	0.20 ± 0.10

the daily MC, correlation with the IMF becomes positive ($P = 0.24 \pm 0.16, S = 0.29 \pm 0.20$) and correlation with SWS drops ($P = 0.00 \pm 0.15, S = -0.02 \pm 0.15$). Similar effects are seen for the MC amplitudes. A positive result is that the long-term indicators of solar activity R SNo. and F10.7 are stable despite the shift–an expected result since these should not modulate the MCs short-term. Correlation of the peak hour and shifted SWVs weakened slightly for the IMF ($r = 0.24 \pm 0.13$) and strengthened slightly for SWS ($r = 0.36 \pm 0.17$). These are the inverted effects from the change in MC amplitude correlation. Overall, the results extracted here are not representative of causal relationships and show that further quantification of atmospheric effects should be done to discern if they are giving rise to spurious correlations with SWVs through the MC data.

4. Conclusions

The strongest result extracted from spectral analysis were the diurnal and semi-diurnal variations, likely from atmospheric modulation of muons. To supplement the FFT, wavelet analysis localized certain frequencies in time. This revealed deformations of the typical signal, that seemed to stretch decreases in MCs over time. These could plausibly have been caused by coinciding space weather events such as geomagnetic storms from impacting CMEs, resulting in characteristic Forbush decreases of CR flux in response. Additionally, spikes in MCs might be due to an optimal alignment of atmospheric conditions. Background radiation levels likely have a significant presence in the MCs as evidenced from both the aliasing in the FFTs and poor quality of the diurnal harmonic fits. Following the methods outlined here, but with finer binning (to make MC closer to a Poisson variable) and more sophisticated removal of background noise (likely due to background radiation sources) may yield more precise results from the FFT, and improve the correlation results of SWVs with MC amplitudes and phase. The correlation analysis with SWVs also is unlikely to yield physically meaningful results unless atmospheric trends are removed from the MCs. Correlations between SWVs, and atmospheric temperature and pressure could also clarify if the strong positive correlations found for MCs with F10.7 and SWS are due to the confounding variables of low pressure and high temperature–conditions which we found correlate with higher MCs. A critical missing piece of the analysis is distinguishing between atmospheric effects and SWV modulation of the MCs.

Further application of the methods in this study to other variables could provide a more comprehensive understanding of short-term CR modulation sources. For example, measures of magnetic activity such as the Kp Index (monitors disturbances caused by solar wind) and Dst Index (a measure of the intensity of Earth's ring current) could help classify short-term fluctuations in MC.

An interesting feature to investigate would be the IMF vector components correlation with MC data arranged in sidereal time to confirm established correlations (Swinson, Regener, and John 1990). Computing the correlation using hourly data instead of daily-averaged data, after also removing atmospheric effects may help clarify the value of the MC time-lag in response to changes in the IMF. Once these correlations are determined, their stability over time can be studied, especially during transient modulation events such as explosive solar activity and geomagnetic storms.

Acknowledgments

This research utilized data from the CosmicWatch project, NASA's OMNI database, Open-Meteo, Meteostat.net, and news from spaceweather.com. The author thanks Dr. Jeffery Spirko and the Honors Program at Texas A&M University-Corpus Christi for guidance and support.

References

Abdullrahman, M., A. H. Hya, and A. Aied (2025). "Exploring daily fluctuations of cosmic ray muon components at a low latitude site and their associations with space weather variables". In: *Journal of Astrophysics and Astronomy* 46.1. DOI: 10.1007/s12036-024-10034-8.

Axani, Spencer N. (2019). *The Physics Behind the CosmicWatch Desktop Muon Detectors*. arXiv: 1908.00146 [physics.ins-det]. URL: https://arxiv.org/abs/1908.00146.

Barbashina, N. S. et al. (2007). "Muon diagnostics of the Earth's atmosphere and magnetosphere". In: *Bulletin of the Russian Academy of Sciences: Physics* 71.7, pp. 1041–1043. DOI: 10.3103/s1062873807070441.

Forbush, S. E. (June 1937). "On the Effects in Cosmic-Ray Intensity Observed During the Recent Magnetic Storm". In: *Phys. Rev.* 51 (12), pp. 1108–1109. DOI: 10.1103/PhysRev.51.1108.3. URL: https://link.aps.org/doi/10.1103/PhysRev.51.1108.3.

Heber, B., T. R. Sanderson, and M. Zhang (1999). "Corotating Interaction Regions". In: *Advances in*

Space Research 23.3, pp. 567–579. DOI: 10.1016/s0273-1177(99)80013-1.

Jokipii, J. R. (1966). "Cosmic-Ray Propagation. I. Charged Particles in a Random Magnetic Field". In: *The Astrophysical Journal* 146, pp. 480–487. DOI: 10.1086/148912.

Lee, Gregory et al. (2019). "PyWavelets: A Python package for wavelet analysis". In: *Journal of Open Source Software* 4.36, p. 1237. DOI: 10.21105/joss.01237.

Mailyan, B. and A. Chilingarian (2010). "Investigation of diurnal variations of cosmic ray fluxes measured with using ASEC and NMDB monitors". In: *Advances in Space Research* 45.11, pp. 1380–1387. DOI: 10.1016/j.asr.2010.01.027.

Mendonça, R. R. De et al. (2013). "Analysis of atmospheric pressure and temperature effects on Cosmic Ray Measurements". In: *Journal of Geophysical Research: Space Physics* 118.4, pp. 1403–1409. DOI: 10.1029/2012ja018026.

Parker, E. N. (1965). "The passage of energetic charged particles through interplanetary space". In: *Planetary and Space Science* 13.1, pp. 9–49. DOI: 10.1016/0032-0633(65)90131-5.

– (1967). "Cosmic Ray Diffusion, Energy Loss, and the Diurnal Variation". In: *Planetary and Space Science* 15.11, pp. 1723–1746. DOI: 10.1016/0032-0633(67)90010-4.

Pomerantz, M. A. and S. P. Duggal (1974). "The sun and cosmic rays". In: *Reviews of Geophysics* 12.3, pp. 343–361. DOI: 10.1029/rg012i003p00343.

Potgieter, M. (2013). "Solar modulation of Cosmic Rays". In: *Living Reviews in Solar Physics* 10. DOI: 10.12942/lrsp-2013-3.

Richardson, I. G. and H. V. Cane (2004). "Identification of interplanetary coronal mass ejections at 1 AU using multiple solar wind plasma composition anomalies". In: *Journal of Geophysical Research: Space Physics* 109.A9. DOI: 10.1029/2004ja010598.

Sharma, S. K. (2008). "18 Cosmic Rays". In: *Atomic and Nuclear Physics*. Pearson Education India.

Swinson, D. B., V. H. Regener, and R. H. St. John (1990). "Correlation of cosmic ray diurnal anisotropies with the interplanetary magnetic field over 21 years". In: *Planetary and Space Science* 38.11, pp. 1387–1398. DOI: 10.1016/0032-0633(90)90114-6.

Virtanen, Pauli et al. (2020). "SciPy 1.0: Fundamental Algorithms for Scientific Computing in Python". In: *Nature Methods* 17, pp. 261–272. DOI: 10.1038/s41592-019-0686-2.